IOP Publishing Journal of Optics
J. Opt. 18 (2016) 095002 (10pp) doi:10.1088/2040-8978/18/9/095002

Does the real part contain all the physical information?

T V Raziman and O J F Martin

Nanophotonics and Metrology Laboratory (NAM), Swiss Federal Institute of Technology Lausanne (EPFL), Lausanne—1015, Switzerland

E-mail: olivier.martin@epfl.ch

Received 12 May 2016, revised 21 July 2016
Accepted for publication 26 July 2016
Published 19 August 2016

Abstract

Polarisation charge formed on nanostructure surfaces upon optical excitation provides a useful tool to understand the underlying physics of plasmonic systems. Plasmonic simulations in the frequency domain typically calculate the polarisation charge as a complex quantity. In this paper, we provide a pedagogical treatment of the complex nature of the polarisation charge and its relevance in plasmonics, and discuss how naively extracting the real part of the complex quantities to obtain physical information can lead to pitfalls. We analyse the charge distributions on various plasmonic systems and explain how to understand and visualise them clearly using techniques such as phase-correction and polarisation ellipse representation, to extract the underlying physical information.

S Online supplementary data available from stacks.iop.org/jopt/18/095002/mmedia

Keywords: surface integral equation, complex numbers, numerical methods, polarisation charge, surface plasmons, plasmonics

(Some figures may appear in colour only in the online journal)

1. Introduction

Electromagnetic simulation methods in the frequency domain incorporate the time-harmonic evolution of various physical quantities by representing them using complex numbers. Although complex numbers are a very useful tool to simplify the mathematics, retrieving the physical information from them can be more conceptually tricky than it appears at first sight. This is especially true in resonant photonic systems, such as plasmonic nanostructures that represent the focus of this article. Indeed, in those systems the optical phase changes as the frequency moves across a resonance. Consequently, taking only the real part of complex quantities and discarding the imaginary part to retrieve the physical relevant observables provides a biased and incomplete description of the system, although this is what one might end up doing by naively following the maxim in electromagnetics textbooks that the real part is the physically relevant quantity.

In this paper, we clarify this misconception by providing a pedagogical treatment of the complex polarisation charge computed by classical electrodynamic simulations in plasmonics. We discuss the information contained in the complex polarisation charge, and the pitfalls associated with naively discarding the imaginary part to retrieve the physically relevant charge. We study plasmonic systems of increasing complexity and describe how the charge on them can be clearly understood and visualised.

Applying an electric field on an object placed in a background of a different dielectric constant induces polarisation charge on the object according to classical electromagnetic theory [1]. If all domains in the system are modelled to have homogeneous dielectric permittivities, the induced charge lies only on the surfaces where permittivity changes abruptly between two domains. Shining light—an electromagnetic wave—on nanostructures thus results in the creation of polarisation charge at the surfaces. The coupling between light and the conduction electrons at metal-dielectric interfaces can give rise to surface electromagnetic excitations known as surface plasmons, which form the foundation of plasmonics [2, 3]. Understanding the charge induced by light on nanostructure surfaces is thus of fundamental interest in plasmonics. Charge on real metal surfaces is typically spread

out over a thickness of a few angstroms [4, 5]. Though the exact nature of the charge spread has an effect on some plasmonic properties, approximating the charge as being located on a zero thickness surface is sufficient for most plasmonic systems and this idealised classical treatment can be employed [4, 6–8]. However, in systems where discreteness of charge and quantum effects become important, a more sophisticated approach would be required [9–11]. Polarisation charge has been used to explain various features in plasmonic systems such as scattering, forces, coupling, second harmonic generation and Fano resonances [12–19].

The simulations in this paper are performed using the surface integral equation (SIE) formulation [20]. Since we are interested in a fundamental treatment, all the simulations have vacuum as the background medium, and the nanostructures are made of gold. The permittivity of gold as a function of frequency ($\tilde{\epsilon}(\omega)$) is given by the Drude formula

$$\tilde{\epsilon}(\omega) = \epsilon_\infty - \frac{\omega_p^2}{\omega(\omega + \mathrm{i}\gamma)}, \tag{1}$$

with Drude parameters $\epsilon_\infty = 9.5$, $\omega_p = 8.95$ eV and $\gamma = 0.0691$ eV to fit the permittivity data from Johnson and Christy [21–23]. The scattering cross section is computed by integrating the Poynting vector of the scattered field on a large sphere surrounding the nanostructure

$$C_{\mathrm{sc}} = \frac{\oint_S \frac{1}{2}\Re[\widetilde{\mathbf{E}}_{\mathrm{scat}} \times \widetilde{\mathbf{H}}^*_{\mathrm{scat}}] \cdot \mathbf{n}\, \mathrm{d}S}{\left| \frac{1}{2}\Re[\widetilde{\mathbf{E}}_{\mathrm{inc}} \times \widetilde{\mathbf{H}}^*_{\mathrm{inc}}] \right|}, \tag{2}$$

where $\widetilde{\mathbf{E}}$ and $\widetilde{\mathbf{H}}$ are the electric and magnetic fields, respectively; and the subscripts scat and inc refer to scattered and incident fields [24]. The polarisation charge density ($\tilde{\sigma}(\mathbf{r})$) at a point on the surface of a domain is evaluated from the discontinuity in the normal component of the electric field

$$\tilde{\sigma}(\mathbf{r}) = \epsilon_0(\widetilde{\mathbf{E}}_{\mathrm{out}}(\mathbf{r}) - \widetilde{\mathbf{E}}_{\mathrm{in}}(\mathbf{r})) \cdot \mathbf{n}, \tag{3}$$

where $\mathbf{n}$ is the outward normal and the subscripts in and out refer to the field inside, respectively outside the domain. The surface fields on the triangles the surface is discretised into for the SIE formulation are evaluated directly from the surface currents to compute the charge [25].

2. Physical meaning of complex polarisation charge

Let us start with a discussion of the physical meaning of the real and imaginary parts of the complex polarisation charge. The first thing that any mathematical textbook states while using the trick of representing a physical quantity by a complex number is that only the real part of the quantity has physical significance, and should be extracted at the end of the calculation. However, we will show here that we should be cautious while applying this rule to the polarisation charge we obtain from the simulations as a complex scalar. The imaginary part of the complex polarisation charge is not an unphysical mathematical tool and should not be discarded.

Why is this? The answer is that we should discard the imaginary part not at the outset but only while computing the charge at a particular instant of time. When we find $\sigma(\mathbf{r}, t)$, the polarisation charge found at a location $\mathbf{r}$ on the structure at a given moment t, we should indeed ensure that it is real. But the output of the simulation $\tilde{\sigma}(\mathbf{r})$ is not merely the polarisation charge at $t = 0$; it contains the entire time evolution of the charge at the location. The surface charge found at a time t can be evaluated as

$$\sigma(\mathbf{r}, t) = \Re[\tilde{\sigma}(\mathbf{r})\exp(-\mathrm{i}\omega t)]. \tag{4}$$

As is evident, the physically relevant charge at an instant is only the real part of the product of the surface charge $\tilde{\sigma}(\mathbf{r})$ and the harmonic propagation term $\exp(-\mathrm{i}\omega t)$. At $t = 0$, this reduces to taking the real part of the complex charge $\tilde{\sigma}(\mathbf{r})$,

$$\sigma(\mathbf{r}, 0) = \Re[\tilde{\sigma}(\mathbf{r})]. \tag{5}$$

However, if we had used only the real part of $\tilde{\sigma}(\mathbf{r})$ on the rhs of (4), we would have found the wrong value of charge at all other values of time t. For example

$$\sigma\left(\mathbf{r}, \frac{T}{6}\right) = \frac{1}{2}\Re[\tilde{\sigma}(\mathbf{r})] + \frac{\sqrt{3}}{2}\Im[\tilde{\sigma}(\mathbf{r})], \tag{6}$$

where T is the time period of the wave. At this instant of time, the value of charge has contributions from both the real and imaginary parts of $\tilde{\sigma}(\mathbf{r})$. In particular, we have

$$\sigma\left(\mathbf{r}, \frac{T}{4}\right) = \Im[\tilde{\sigma}(\mathbf{r})]. \tag{7}$$

That is, only the imaginary part of $\tilde{\sigma}(\mathbf{r})$ contributes to $\sigma(\mathbf{r}, t)$ at this instant. Had we discarded the imaginary part of $\tilde{\sigma}(\mathbf{r})$ in the beginning, we would have found the incorrect result of zero instead.

This brings us to the next point, what does time t mean in such a system where all the fields and the charge have a harmonic dependence? The answer is that usually, the zero point of time is implicitly defined by the illumination conditions. For example, suppose that we simulate the response of our structure for plane wave illumination defined by the complex electric polarisation vector $\widetilde{\mathbf{E}}(\mathbf{r}) = \widetilde{\mathbf{E}}_{\mathbf{0}}\exp(\mathrm{i}\mathbf{k}\cdot\mathbf{r})$. Just as in the case of charge, the complex valuedness of the electric field vector contains the information about its time evolution. The instantaneous value of the electric field vector at a location is given by $\mathbf{E}(\mathbf{r}, t) = \Re[\widetilde{\mathbf{E}}(\mathbf{r})\exp(-\mathrm{i}\omega t)] = \Re[\widetilde{\mathbf{E}}_{\mathbf{0}}\exp(\mathrm{i}\mathbf{k}\cdot\mathbf{r} - \mathrm{i}\omega t)]$. Through this definition, we have implicitly defined the zero of time with respect to the oscillation of the incident electric field, by setting $\mathbf{E}(\mathbf{0}, 0) = \Re[\widetilde{\mathbf{E}}_{\mathbf{0}}]$. This is a general feature of linear harmonic problems—since all excitations and responses in the problem are purely oscillatory, $t = 0$ has no physical significance and has to be set explicitly, allowing us to choose it to our convenience.

If we now subtract a phase ϕ from the electric field

$$\widetilde{\mathbf{E}}_\phi(\mathbf{r}) = \widetilde{\mathbf{E}}_{\mathbf{0}}\exp(-\mathrm{i}\phi)\exp(\mathrm{i}\mathbf{k}\cdot\mathbf{r}), \tag{8}$$

the simulation results would be identical except for all the fields and the charge getting the additional phase factor of

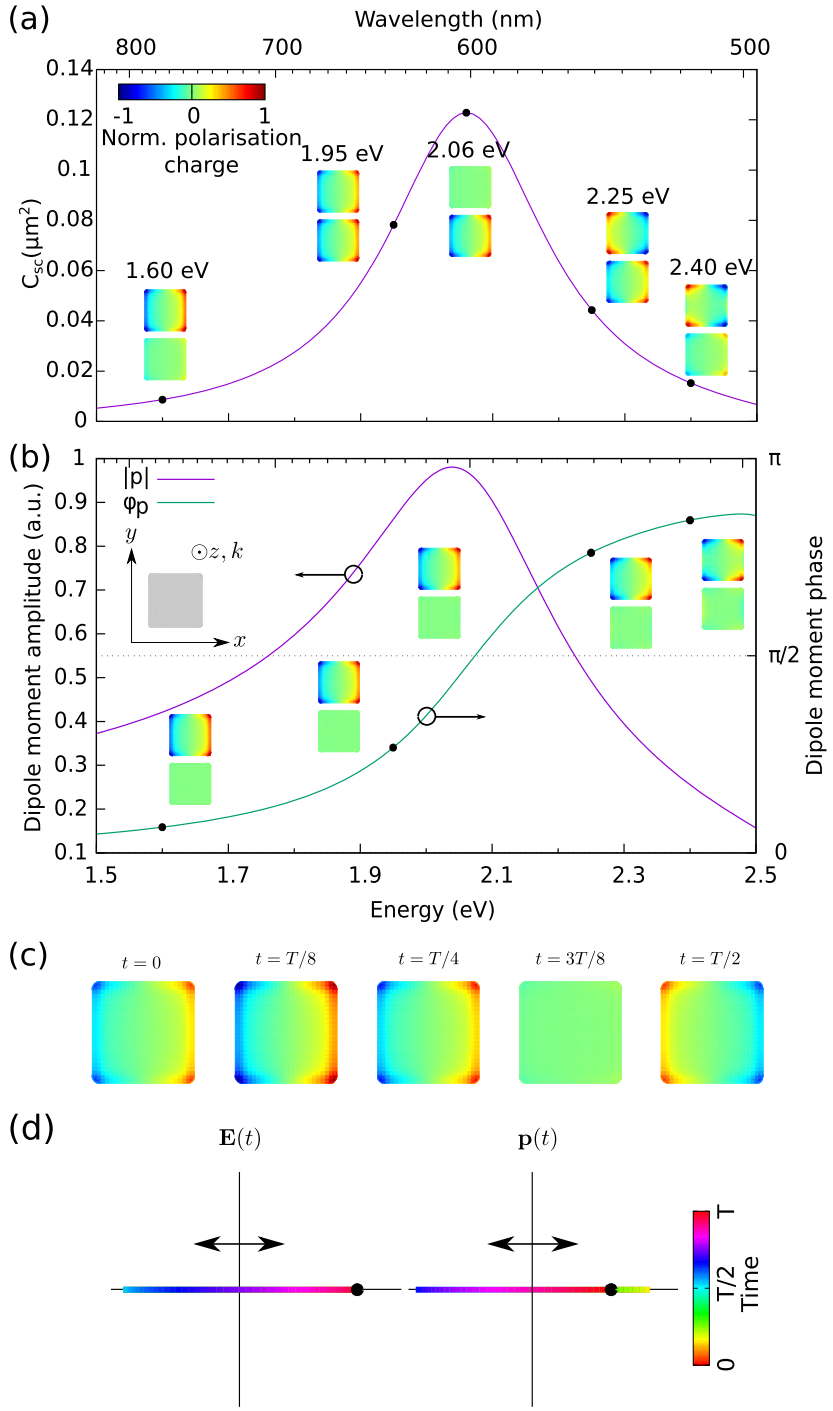

Figure 1. (a) Scattering cross section of the 120 nm × 120 nm × 40 nm nanosquare (shown in the inset of (b)) for incident light polarised along the x-axis, and real (top) and imaginary (bottom) parts of the polarisation charge $\tilde{\sigma}(\mathbf{r})$ at five chosen frequencies. (b) Amplitude and phase of the dipole moment, and the polarisation charge in (a) phase-corrected to the respective dipole moments. (c) Instantaneous charge $\sigma(\mathbf{r}, t)$ for 1.95 eV at five different times, and (d) the curve traced by the instantaneous incident electric field and dipole moment vectors over a period for the same frequency. The black dot indicates the time $t = 0$, and the time evolution is colour-coded from red to green to blue to red. (An animation of this figure is available in the supplementary data.)

$-\phi$. This is equivalent to advancing in time by $\frac{T\phi}{2\pi}$, and does not change the physics in any way. Phase subtraction results in an advancement in time due to the fact that the harmonic dependence is defined as $\exp(-\mathrm{i}\omega t)$—had we used the $\exp(\mathrm{i}\omega t)$ convention, it would have resulted in a time lag instead. Something slightly different happens when we find the modes of the system instead of the response to certain illumination. In this case, there is automatically the freedom to multiply the fields and the charge by an arbitrary phase since the incident illumination is zero [26].

Since the zero of time has been shown to be arbitrary, we have the freedom to redefine it as we see fit to suit our

convenience. As explained above, this is identical to subtracting a phase from all the fields and the charge. Subtracting phase ϕ from the charge, we have

$$\tilde{\sigma}_{\phi}(\mathbf{r}) = \tilde{\sigma}(\mathbf{r})\exp(-\mathrm{i}\phi). \tag{9}$$

Although the values of the real and imaginary parts of charge will change with this, (4) will still be valid. Such phase/time shifts can be used to change the phase of the charge distribution and move the imaginary part of the charge to the real part without any loss of information. As will be shown later, using such shifts—which we will henceforth refer to by the term 'phase-correction'—can help better understand the charge distribution on some systems. However, care must be taken to ensure that the charge everywhere (and fields, if they are being used) are propagated by the same phase/time delay simultaneously. It is incorrect to apply phase-correction to the charge on one part of the system while leaving another part unchanged. This could result in unphysical results such as net charge on free standing structures.

With this introduction, we hope that the physical meaning of the complex charge is clear. We now move on to analysing a few systems of increasing complexity to see how best to study the charge on these systems and to understand various nuances.

3. Results and discussion

3.1. Nanosquare

We first consider a simple system consisting of a nanosquare of dimensions 120 nm × 120 nm × 40 nm. The nanosquare is placed on the *xy*-plane and illuminated by a plane wave propagating along z and polarised along x.

The scattering cross section of the nanosquare is shown in figure 1(a). There is a single scattering peak in the frequency range considered, corresponding to the dipole resonance. The complex polarisation charge at five different frequencies induced on the surface are also shown. Note that for each wavelength, the real (top) and imaginary (bottom) parts of the complex polarisation charge are normalised together to the maximum value of both of them over the whole surface, such that the evolution of the charge distribution is clearly visible. At low frequencies, it is seen that the real part of the charge dominates over the imaginary part. As the frequency is increased, the imaginary part becomes more and more significant, and looks similar to the real part. Near the resonance peak, the imaginary part dominates the real part. Once the scattering peak is crossed, the real part picks up strength again, though it gains a sign flip as well. Far away from the resonance, we have again the situation where the real part dominates the imaginary part. The nanosquare at resonance is a good example of a system in which taking only the real part of the charge at the outset would have given a completely incorrect picture—that would have resulted in zero charge at the scattering peak, where the charge has not vanished but only shifted in phase.

The behaviour of real and imaginary parts of the charge is similar to that seen in simple harmonic motion, since the system is similar to a classical driven oscillator [27–31]. This parallel becomes more clear on looking at the dipole moment induced on the square [1]. The dipole moment $\tilde{\mathbf{p}}$ is computed from the position moment of the polarisation charge

$$\tilde{\mathbf{p}} = \oint_{S} \mathbf{r}\,\tilde{\sigma}(\mathbf{r})\,\mathrm{d}S, \tag{10}$$

where S is the surface of the nanosquare. The normalised amplitude and phase of the x-component of the dipole moment are shown in figure 1(b). The phase of the dipole moment shows a smooth transition from 0 to π, passing through $\pi/2$ near the scattering peak. This is the typical behaviour in resonant systems, where the response starts to show a lag with respect to the driving force on nearing the resonance, changing from in-phase at low frequencies to out-of-phase at high frequencies. The phase of the dipole moment thus tells us how much the charge distribution lags behind the incident field. This can be seen more clearly by looking at the time-evolution of the charge. The charge for 1.95 eV is animated in Visualisation 1, and snapshots are provided in figure 1(c). The charge magnitude is seen to peak near $t = T/8$, which matches the dipole moment phase of approximately $\pi/4$. The curves showing the evolution of the instantaneous incident field ($\mathbf{E}(t)$) and the dipole moment vector ($\mathbf{p}(t)$) for the same frequency plotted in figure 1(d) also demonstrate the phase lag. The colours in figure 1(d) denote the time, with evolution from red to green to blue to red, and $t = 0$ is marked with the black dot. Both the electric field and the dipole moment lie on the horizontal line, but the phase lag is evident from the different positions of the black dot. Note that only half the time evolution is visible in the curves because of the back-and-forth oscillation.

As explained in the previous section, subtracting a phase from the incident field does not change the physics but modifies the charge by the same phase. Since the phase of the charge is formed due to the charge lagging behind the electric field, we can offset it by applying an equal phase-correction. For each of the five frequencies shown earlier in figure 1(a), we subtract the phase of the dipole moment at the corresponding frequency from the incident field and thus from the charge using (8) and (9), and plot the real and imaginary parts of the phase-corrected charge in the inset of figure 1(b). With this phase-correction, we see that the imaginary part has vanished almost entirely. This is a signature of the system having a single dominant mode, since the presence of a second mode with a different phase would have resulted in non-vanishing imaginary part. In such simple systems, phase-correction allows us to move all the information of the charge to the real part and thus discard the imaginary part.

Due to the symmetry in the system, y-polarised light will result in the same scattering cross section. The charge induced will be identical in magnitude and phase too, except for being rotated by 90°. The situation becomes more interesting when, instead of x- or y-polarisations, the incident wave polarisation is a linear combination of the two. A general input

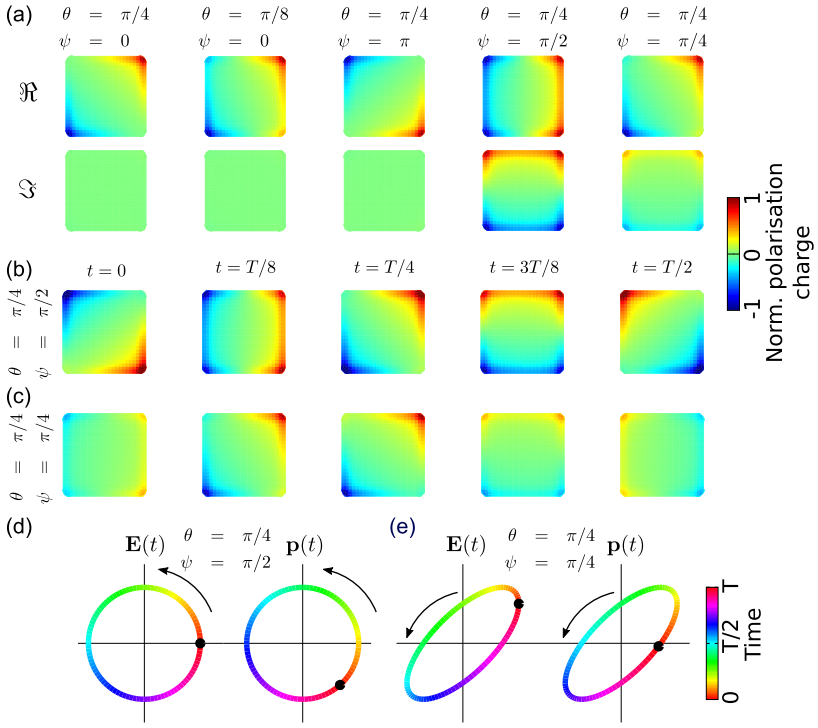

Figure 2. (a) Real (top) and imaginary (bottom) parts of polarisation charge for various linear combinations of x- and y-polarised incidences based on (11). The charge plots have been phase-corrected to the phase of the dipole moment, see text. (b) Instantaneous charge plots at five different times shown without phase-correction for ($\theta = \pi/4$, $\psi = \pi/2$), and (c) for ($\theta = \pi/4$, $\psi = \pi/4$). The curve traced by the tip of the incident electric field and the dipole moment vectors over a period are plotted for these two cases in (d) and (e), respectively. (An animation of this figure is available in the supplementary data.)

polarisation can be represented by

$$\widetilde{\mathbf{E}}_{\mathbf{0}}(\theta, \psi) = \cos(\theta)\,\hat{x} + \sin(\theta)\exp(\mathrm{i}\psi)\,\hat{y}. \qquad (11)$$

It is easy to see that all linear, circular and elliptical polarisations can be described by suitable values of θ and ψ. To study the charge induced by general polarisation states, we fix the input frequency to be 1.95 eV. The real and imaginary parts of charge for certain values of θ and ψ are shown in figure 2(a). Note that in all these cases, the charge is phase-corrected using the phase of the x-component of the dipole moment as before.

When the relative phase ψ between the x- and y-components of input polarisation is zero, we see that the imaginary part of the phase-corrected charge plots is zero. This should not be surprising since the phase-correction sets the imaginary part of charge for both x- and y-polarisations to zero and we are merely looking at a linear combination of both without additional phase offsets. Changing the value of θ changes the real part of the charge distribution—the charge essentially gets rotated by θ. Adding a phase offset of $\psi = \pi$ retains these features since it merely adds a negative sign to one of the components.

However, the situation changes when the phase offset ψ is nontrivial. When $\theta = \pi/4$ and $\psi = \pi/2$, we see from figure 2(a) that the real and imaginary parts have equal magnitude. Since they are geometrically rotated by 90°, no phase-correction can result in the vanishing of one part, a situation unlike what has been discussed till now. To understand what is going on, we can look at the time evolution of the charge $\sigma(\mathbf{r}, t)$. The surface charge is animated as a function of time in Visualisation 2, and snapshots at five instants are shown in figure 2(b). At $t = 0$, the charge distribution is such that the dipole moment is diagonal. With increasing time, the charge shifts: the positive charge found at the bottom right corner of the square migrates towards the positive y-direction, whereas the negative charge at the top left corner does the reverse. This results in a rotation of the dipole moment. At $t = T/4$, the charge has reoriented such that the dipole moment is now along the other diagonal. This rotation continues further with time. This should not be surprising, since $\widetilde{\mathbf{E}}_{\mathbf{0}}(\theta = \pi/4, \psi = \pi/2) = (\hat{x} + \mathrm{i}\hat{y})/\sqrt{2}$ is circularly polarised illumination. The evolution of the incident electric field and the instantaneous dipole moment as a function of time are plotted in figure 2(d). It can be seen that the dipole moment curve is identical to the incident field curve, except for a rotation along the colours. This geometrical similarity is the consequence of the polarisability along x- and y-directions being identical, and the colour rotation between $\mathbf{E}(t)$ and $\mathbf{p}(t)$ is due to the phase lag between incident light and the dipole moment. The rotation of the dipole moment clearly explains the trends seen in the time evolution of the charge. This example reiterates the importance of keeping both real and imaginary parts of the charge, since it is impossible to explain the rotation of charge using only one of them. It also becomes clearer that no phase-correction will help us in this case because there is no instant of time at which the charge vanishes (Visualisation 2/figure 2(b)) and

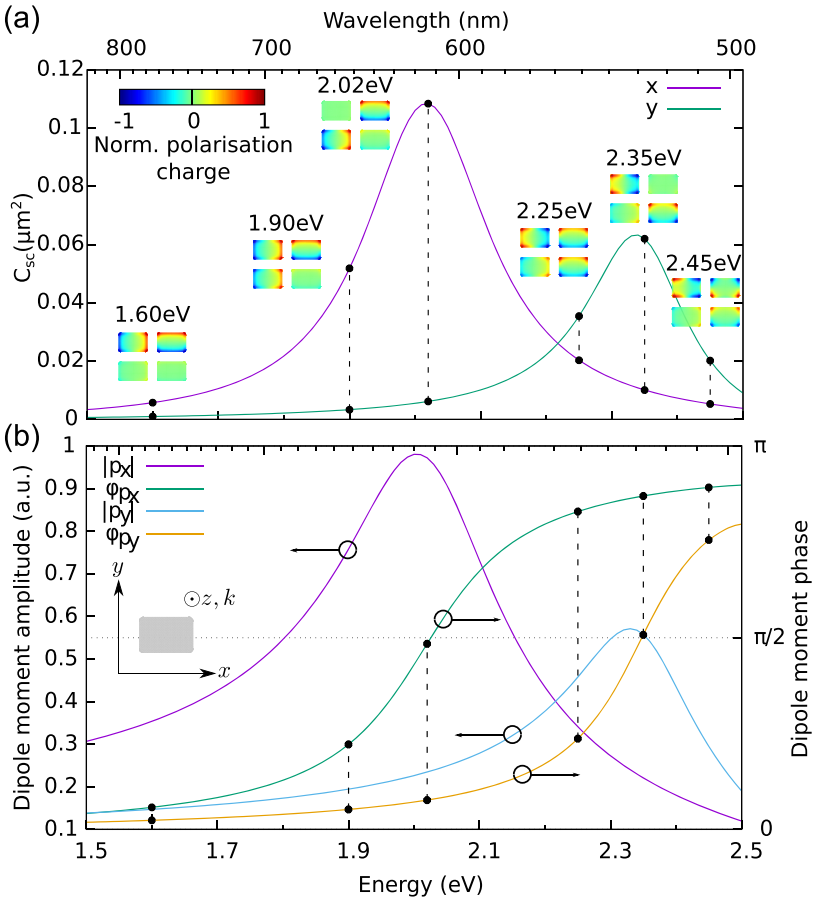

Figure 3. (a) Scattering cross section of the 120 nm × 80 nm × 40 nm nanorectangle (shown in the inset of (b)) for *x*- and *y*-polarised illuminations. Real (top) and imaginary (bottom) parts of the polarisation charge are also shown for *x*- (left) and *y*- (right) polarised incidence for selected frequencies. (b) Amplitude and phase of the induced dipole moments.

the dipole moment curve does not pass through the origin (figure 2(d)).

When ψ is changed to $\pi/4$, the situation changes tremendously. The instantaneous charge for this case has been plotted in figure 2(c). The rotation of the dipole moment is no longer uniform. For example, between $t = 3T/8$ and $t = T/2$, the instantaneous dipole moment rotated 90° from $+y$ direction to $-x$ in a duration of $T/8$, in contrast with the $\psi = \pi/2$ case which always took $T/4$ time for rotating the dipole moment by 90°. The reason for this can be understood by looking at the $\mathbf{E}(t)$ and $\mathbf{p}(t)$ curves in figure 2(e). The incident field is now elliptical, with major axis inclined to the symmetry axes of the square. As a result, so is the dipole moment. The incident electric field does not rotate with a constant angular velocity, as can be observed from the colours on the ellipse. This results in a time-varying rotation of the dipole moment as well. The phase difference between incident field and dipole moment also means that their instantaneous rotations have different rates.

This example goes on to show that, though the real and imaginary parts of the charge contain the full information about the evolution of polarisation charge on the structure, visualising the evolution is not straightforward. In situations where a single mode is dominantly excited by the incident light, phase-correction permits to move all the information in the charge to the real part for a given frequency—but even in the simple scenario where two degenerate modes are excited with difference phases by the incident field, phase-correction cannot make the imaginary part vanish. Additional tools such as movies and snapshots of charge at different times, and dipole moment ellipses as we proposed here, make it easier to grasp the complexity of the charge evolution.

3.2. Nanorectangle

Next, we break the symmetry of the nanosquare by turning it into a rectangle. The nanorectangle has dimensions 120 nm × 80 nm × 40 nm. The width of 80 nm ensures that the polarisability along *y*-direction is comparable to that along *x* in the frequency range being considered. As a result, the system has two resonances for the two orthogonal polarisations, but the resonances are sufficiently close in terms of peak intensity and position for them to have significant overlap.

The scattering cross section for *x*- and *y*-incident polarisations are plotted in figure 3(a) along with the real and imaginary polarisation charge for both incidence conditions at six chosen frequencies. It is clear that the relation between real and imaginary parts of charge for each frequency is

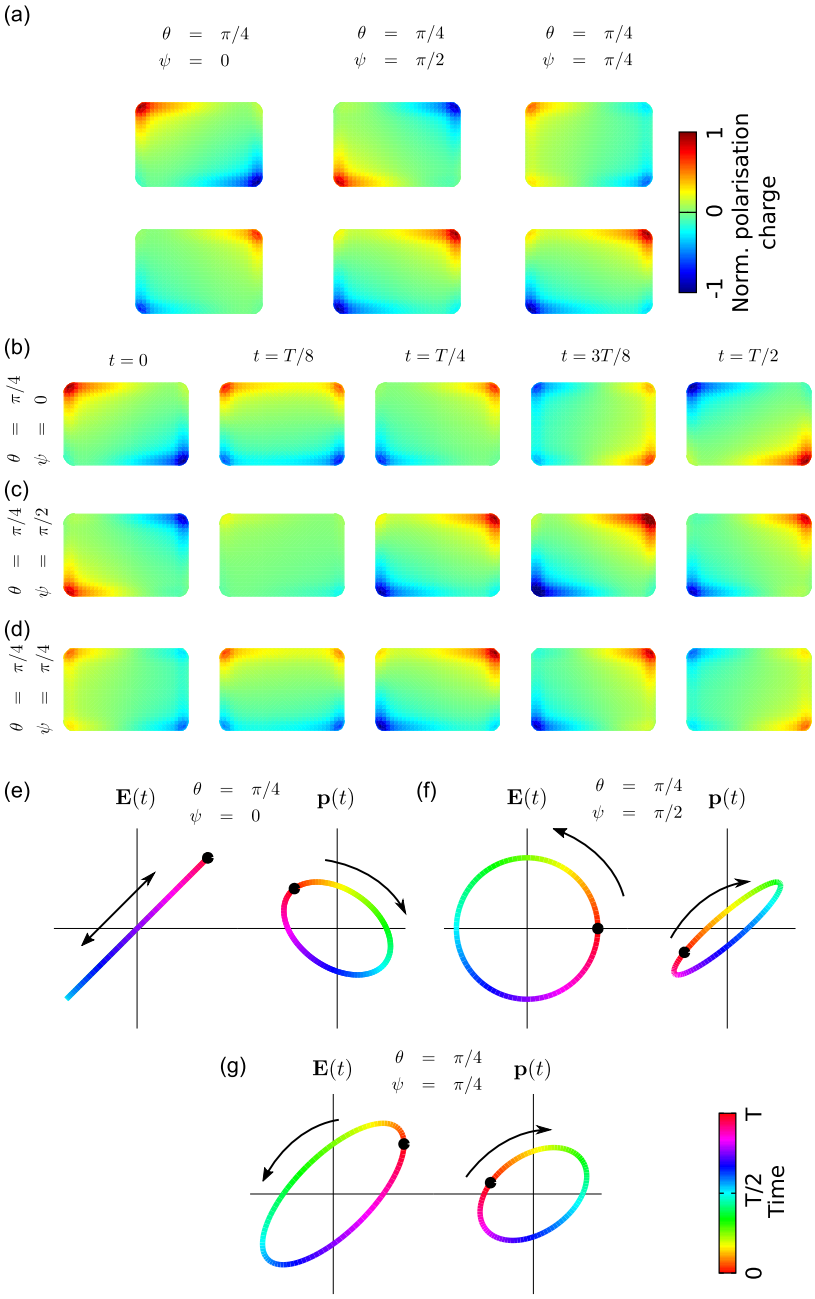

Figure 4. (a) Real and imaginary parts of polarisation charge without phase-correction at 2.20 eV for three different incident conditions corresponding to θ and ψ values indicated in the figure. (b)–(d) Instantaneous charge plots at five different times for the three illuminations in (a). (e)–(g) Curves traced by the incident electric field and dipole moment vectors over a time period for the three illuminations. The black dot indicates the time $t = 0$, and the time evolution is colour-coded from red to green to blue to red.

completely different for the two polarisations. The reason for this can be seen from the dipole moment amplitude and phase for the two different polarisations, plotted in figure 3(b). Not only is the phase of the two dipole moments different, the phase difference between the two is not a constant either. This is a consequence of the scattering peaks being frequency separated. As a result, it is not possible to simultaneously phase-correct the charge plots for x- and y-polarised incidence at a given frequency to let the imaginary parts of both vanish. We see once again that considering only the real part of the charge distribution would have led us to wrong conclusions especially about the relative magnitudes of the charge (and thus the dipole moments), and the phase difference between the x- and y-responses.

Next, as done previously, we look at the charge on the structure arising from combinations of x- and y-polarisations using (11). The frequency is fixed at 2.20 eV since the polarisability along both directions is nearly equal in magnitude. The real and imaginary parts of charge for $\theta = \pi/4$ for three different values of ψ are plotted in figure 4(a). Note that no phase-correction has been done on any of the images in this set.

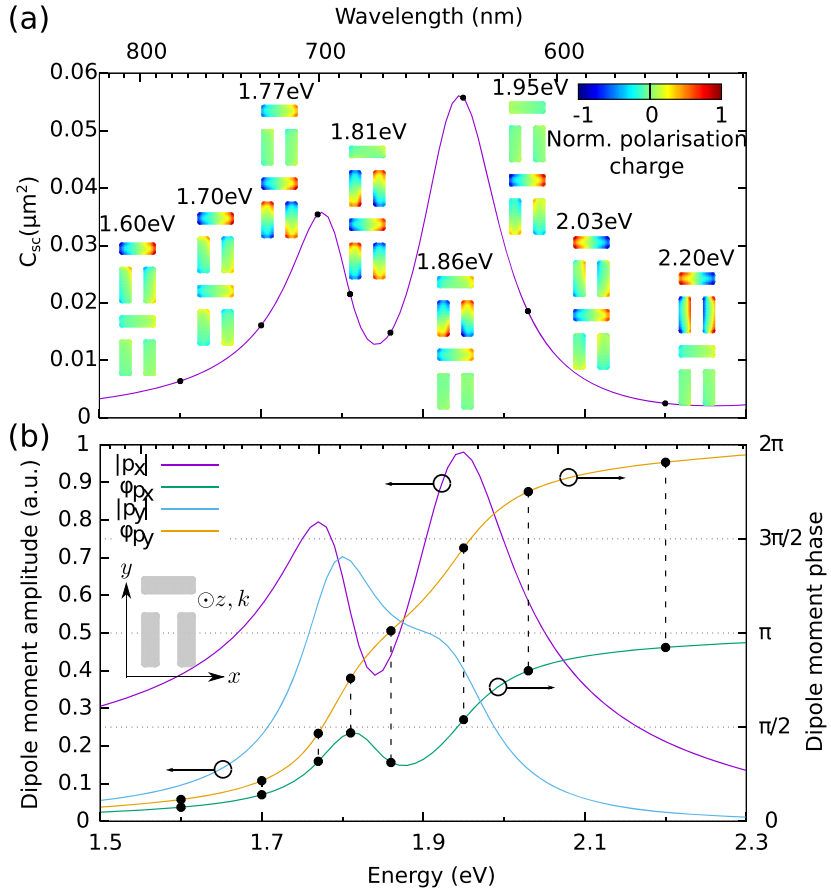

Figure 5. (a) Scattering cross section of the dolmen (shown in the inset of (b)) for x-polarised incidence, and real and imaginary parts of the polarisation charge at eight different frequencies. (b) Amplitude and phase of the x-component of the dipole moment of the horizontal arm and y-component of the dipole moment of the left vertical arm.

The first thing to note is that even when $\psi = 0$, the imaginary part of the charge does not vanish. It is also geometrically different from the real part, implying that no phase-correction can fix it, as expected. The time evolution of the charge, plotted in figure 4(b), shows that the surface charge rotates with time. This is a consequence of the complex polarisability of the rectangle along x and y being different. Figure 4(e) compares the evolution of the incident electric field and dipole moment vectors, and it is evident that the two are not similar anymore unlike the case of the nanosquare. Though the input polarisation curve is a straight line, the dipole moment curve is an ellipse with the minor axis comparable to the major axis. The nanorectangle is thus able to convert linearly polarised incident field into partly circularly polarised scattered field. Since the ellipse does not pass through the origin, there is no instant at which the dipole moment and hence the charge vanishes—reiterating that it is impossible to phase-correct the charge to have only the real part. Both the real and imaginary parts of $\tilde{\sigma}(\mathbf{r})$ are thus important.

For $\psi = \pi/2$, the real and imaginary parts of charge look similar except for a sign flip. This is the signature of the polarisation charge on the structure being linear. This can be observed in the time evolution plotted in figure 4(c). The charge seems to wax and wane rather than move about the structure. Looking at the incident field and dipole moment plots in figure 4(f) explains why: though the incident field moves in a circle, the dipole moment is an ellipse with a very short minor axis, so that the dipole moment nearly moves in a line with time. $\psi = \pi/4$ gives an intermediate situation, where both the incident field and the dipole moment are elliptical (figures 4(d) and (g)). Furthermore, it is interesting to note that the two ellipses have opposite senses of rotation. The colours on the two ellipses are flipped, and the dipole moment rotates clockwise while the incident polarisation rotation is anticlockwise. This interesting behaviour arises from the large phase difference ($>\frac{\pi}{2}$) between the dipole moments along x and y. Since the magnitudes of the dipole moments along x and y are nearly equal for the frequency under consideration, this means that polarisabilities along the two directions are almost negatives of each other. As a result, the dipole moment ellipse is flipped with respect to the incident field ellipse and the sense of rotation is reversed. It should be noted that rotation of the dipole moment gets transmitted to the far field as circular polarisation in the scattered field. Nanostructures like the nanorectangle which have polarisabilities along the two axes with similar magnitudes but large phase differences can achieve a relative rotation between incident field and induced dipole moment as

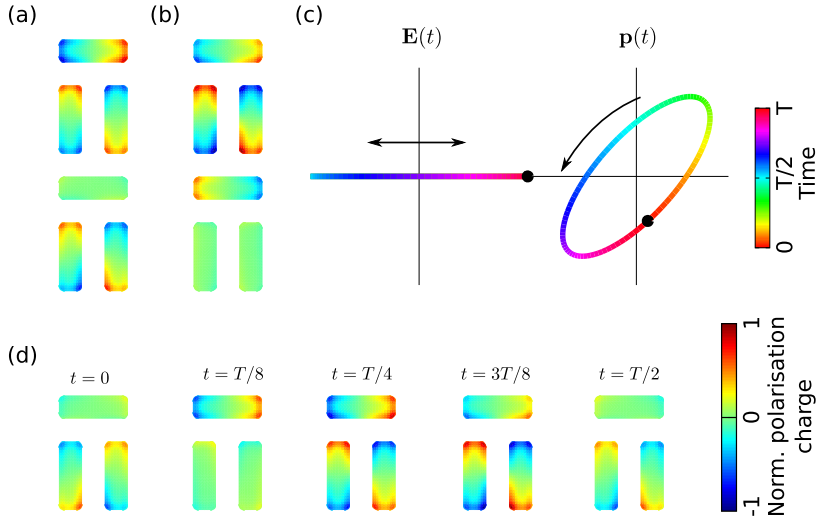

Figure 6. (a) Real and imaginary parts of the charge plots at 1.80 eV after phase-correction to the horizontal arm. (b) Same as (a), but phase-corrected to the vertical arm. (c) Curves traced by the incident electric field, and the sum of the x-component of the dipole moment of the horizontal arm and the y-component of the left vertical arm. (d) Time evolution of the instantaneous charge plots. (An animation of this figure is available in the supplementary data.)

described above, and thus be used as polarisation converters [32, 33].

3.3. Dolmen

The next structure we analyse is the dolmen, a system of considerable interest to the plasmonic community due to the Fano resonance arising from the interaction between the dipole mode supported by the horizontal arm and the quadrupole mode supported by the vertical arms [34–45]. Both the horizontal arm and the vertical arms of the dolmen have dimensions 120 nm × 40 nm × 40 nm. The scattering cross section for incident polarisation along the horizontal arm and real and imaginary parts of the polarisation charge for selected frequencies are plotted in figure 5(a).

The scattering cross section shows the features of a Fano resonance, with two scattering peaks and a scattering dip. As the frequency is increased, the charge on the horizontal arm behaves in a similar fashion as the nanosquare shown in figure 1(a). At low frequencies, the real part of the charge is dominant. With increasing frequency, the imaginary part takes over, after which the real part becomes dominant again. The behaviour of the vertical arm is more interesting. The charge on the vertical arms changes from real to imaginary to real twice. This can be seen more clearly in the dipole moment plot in figure 5(b). The amplitude of the dipole moment along x-direction for the horizontal arm and y-direction for the left vertical arm are shown (the right vertical arm has charge opposite to the left). The phase of the dipole moment of the horizontal arm changes from 0 to π as usual. But the vertical arm phase changes from 0 to 2π. This is due to the fact that the mode of the system changes from bonding to antibonding across the Fano resonance. The charge distributions on the horizontal and vertical bars across the gap are attractive at low frequencies but repulsive at high frequencies [46]. The dipole moment of the vertical bars thus gets an additional sign flip relative to the horizontal bar (which is being fed by the incident field directly and thus gains a phase of π across the resonance), resulting in a total phase change of 2π. The emergence of the short-axis resonance of the vertical arms can also be observed at high frequencies.

The phase difference between the charge distributions on the horizontal and vertical arms means that simultaneous phase-correction is impossible in this case as well. The real and imaginary parts of the charge plots corrected to the dipole moment phase of the horizontal and vertical arms are shown in figures 6(a) and (b) respectively for 1.80 eV. Correcting the charge plots by the dipole moment phase of the horizontal arm indeed results in the vanishing of the imaginary part of the charge on the horizontal arm, but it remains on the vertical arm. On applying phase-correction using the dipole moment of the vertical arm, the reverse happens. This shows that in coupled systems, taking a snapshot of charge at any single instant does not give the complete information about the charge evolution, even for simple incidence conditions. In particular, phase-correction to completely vanish the imaginary part of the charge everywhere is not possible even for x-polarised incidence, a situation unlike the systems described previously.

The evolution of charge on the dolmen with time has been shown in Visualisation 3, with snapshots presented in figure 6(d). It is evident that though the charge evolutions of both the horizontal arm and the vertical arm are similar, they do not happen in-phase. This phase difference can be visualised also through the incident field and dipole moment evolution curves shown in figure 6(c). Note that the dipole moment shown is the sum of the x-component of the dipole moment of the horizontal arm and the y-component of the dipole moment of the left vertical arm. This is not the net dipole moment of the system, but provides maximum information about the charge distribution—the other component of dipole moment on each arm is much smaller in magnitude,

and the *y*-component of the dipole moment on the right vertical arm is just the negative of that on the left arm. The dipole moment ellipse has major axis at nearly 45°, and the aspect ratio is not too high. This is a result of the dipole moments of both arms being nearly equal in magnitude, and the phase difference between them being significant. Once again, had we extracted only the real part from the charge at the outset, we would not have been able to notice the phase difference.

4. Conclusion

We have shown how both the real and imaginary parts of the complex polarisation charge are relevant, and taking only the real part results in a misleading interpretation of physical phenomena. Physical features like geometric migration of charge and phase difference between parts of compound systems cannot be analysed from the real part of the charge alone. The complex nature of the charge and their increasingly complicated behaviour in systems possessing multiple modes and asymmetry makes it tricky to extract relevant physical information from them. We have studied different plasmonic systems and shown how techniques such as phase-correction and polarisation ellipse representation help to visualise the charge and understand the respective structures better.

Acknowledgments

Funding from the Swiss National Science Foundation (Project 200020_135452) is gratefully acknowledged.

References

[1] Jackson J D 1998 *Classical Electrodynamics* 3rd edn (New York: Wiley)
[2] Maier S A 2007 *Plasmonics: Fundamentals and Applications* (Berlin: Springer)
[3] Stockman M I 2011 *Opt. Express* **19** 22029–106
[4] Lang N D and Kohn W 1973 *Phys. Rev.* B **7** 3541–50
[5] Tsuei K D, Plummer E, Liebsch A, Pehlke E, Kempa K and Bakshi P 1991 *Surf. Sci.* **247** 302–26
[6] Feibelman P J 1982 *Prog. Surf. Sci.* **12** 287–407
[7] Tsuei K D, Plummer E W and Feibelman P J 1989 *Phys. Rev. Lett.* **63** 2256–9
[8] Feibelman P J 1989 *Phys. Rev.* B **40** 2752–6
[9] Ekardt W 1985 *Phys. Rev.* B **31** 6360–70
[10] Zuloaga J, Prodan E and Nordlander P 2010 *ACS Nano* **4** 5269–76
[11] Esteban R, Borisov A G, Nordlander P and Aizpurua J 2012 *Nat. Commun.* **3** 825
[12] Kottmann J P, Martin O J F, Smith D R and Schultz S 2000 *New J. Phys.* **2** 27
[13] Kottmann J P and Martin O J 2001 *Opt. Express* **8** 655–63
[14] Davis T J, Vernon K C and Gómez D E 2009 *Phys. Rev.* B **79** 155423
[15] Ye J, Dorpe P V, Lagae L, Maes G and Borghs G 2009 *Nanotechnology* **20** 465203
[16] Fan J A, Wu C, Bao K, Bao J, Bardhan R, Halas N J, Manoharan V N, Nordlander P, Shvets G and Capasso F 2010 *Science* **328** 1135–8
[17] Ginzburg P, Krasavin A, Sonnefraud Y, Murphy A, Pollard R J, Maier S A and Zayats A V 2012 *Phys. Rev.* B **86** 085422
[18] Raziman T V and Martin O J F 2013 *Opt. Express* **21** 21500–7
[19] Raziman T V and Martin O J F 2015 *Opt. Express* **23** 20143–57
[20] Kern A M and Martin O J F 2009 *J. Opt. Soc. Am.* A **26** 732–40
[21] Johnson P B and Christy R W 1972 *Phys. Rev.* B **6** 4370–9
[22] Oubre C and Nordlander P 2004 *J. Phys. Chem.* B **108** 17740–7
[23] Etchegoin P G, Le Ru E C and Meyer M 2006 *J. Chem. Phys.* **125** 164705
[24] Kern A and Martin O J F 2010 *IEEE Trans. Antennas Propag.* **58** 2158–61
[25] Ji A, Raziman T V, Butet J, Sharma R P and Martin O J F 2014 *Opt. Lett.* **39** 4699–702
[26] Bernasconi G D, Butet J and Martin O J 2016 *J. Opt. Soc. Am.* B **33** 768–79
[27] Abelès F 1976 *Surf. Sci.* **56** 237–51
[28] Grigorenko A N, Nikitin P I and Kabashin A V 1999 *Appl. Phys. Lett.* **75** 3917–9
[29] Joe Y S, Satanin A M and Kim C S 2006 *Phys. Scr.* **74** 259–66
[30] Kats M A, Yu N, Genevet P, Gaburro Z and Capasso F 2011 *Opt. Express* **19** 21748–53
[31] Zuloaga J and Nordlander P 2011 *Nano Lett.* **11** 1280–3
[32] Abasahl B, Dutta-Gupta S, Santschi C and Martin O J F 2013 *Nano Lett.* **13** 4575–9
[33] Abasahl B, Santschi C and Martin O J F 2014 *ACS Photon.* **1** 403–7
[34] Zhang S, Genov D A, Wang Y, Liu M and Zhang X 2008 *Phys. Rev. Lett.* **101** 047401
[35] Verellen N, Sonnefraud Y, Sobhani H, Hao F, Moshchalkov V V, Dorpe P V, Nordlander P and Maier S A 2009 *Nano Lett.* **9** 1663–7
[36] Luk'yanchuk B, Zheludev N I, Maier S A, Halas N J, Nordlander P, Giessen H and Chong C T 2010 *Nat. Mater.* **9** 707–15
[37] Gallinet B and Martin O J F 2011 *Opt. Express* **19** 22167–75
[38] Zhang Q, Xiao J J, Zhang X M, Yao Y and Liu H 2013 *Opt. Express* **21** 6601–8
[39] Zhang Q and Xiao J J 2013 *Opt. Lett.* **38** 4240–3
[40] Gallinet B and Martin O J F 2013 *ACS Nano* **7** 6978–87
[41] Butet J and Martin O J F 2014 *Nanoscale* **6** 15262–70
[42] Butet J and Martin O J F 2014 *ACS Nano* **8** 4931–9
[43] Li Z, Zhang S, Tong L, Wang P, Dong B and Xu H 2014 *ACS Nano* **8** 701–8
[44] Yan C and Martin O J F 2014 *ACS Nano* **8** 11860–8
[45] Chen H, Liu S, Zi J and Lin Z 2015 *ACS Nano* **9** 1926–35
[46] Gallinet B and Martin O J F 2011 *ACS Nano* **5** 8999–9008